THE JOURNAL OF COMPARATIVE NEUROLOGY 292:480–494 (1990)

Developmental Changes in the Distribution of Retinal Catecholaminergic Neurones in Hamsters and Gerbils

JOHN MITROFANIS AND BARBARA L. FINLAY
Department of Anatomy, University of Sydney, Australia (J.M.); Department of Psychology, Cornell University, Ithaca, NY (B.L.F.)

ABSTRACT

Although Syrian hamsters and Mongolian gerbils are closely related, they have quite different patterns of retinal ganglion cell distribution and different patterns of retinal growth that produce their distributions. We have examined the morphology and distribution of catecholaminergic (CA) neurones in adult and developing retinae of these species in order to gain a more general understanding of the mechanisms producing cellular topographies in the retina. CA neurones were identified with an antibody to tyrosine hydroxylase (TH), the rate limiting enzyme in the production of catecholamines.

In adult retinae of both hamsters and gerbils, most CA somata were located in the inner part of the inner nuclear layer (INL) and CA dendrites spread in a outer stratum of the inner plexiform layer (IPL). Their somata varied with retinal position, being largest in temporal and smallest in central retina. In hamsters, but not gerbils, a small number of CA interplexiform cells was also observed. In development, CA somata of hamster retinae were observed first in the middle and/or scleral regions of the cytoblast layer (CBL) at P (postnatal day) 8. By P12, CA somata were commonly located in the inner part of the INL and their dendrites spread into the outer region of the IPL. In developing gerbil retinae, CA somata were first observed at P6 in the middle of the CBL. Over subsequent days, they migrated into the inner part of the INL and spread their dendrites into the outer strata of the IPL.

In both hamsters and gerbils, CA cells were initially concentrated in the superior temporal margin of the retina. In hamsters, this supero-temporal concentration persisted until adulthood, whereas in adult gerbils, the greatest density of CA cells was found just superior to the visual streak. These distributions were distinct from those of the ganglion cells in adult and developing retinae of each species. We discuss the role of maturational expression of TH, cell death, and retinal growth in the generation of the distinct distribution of the CA cells.

Key words: amacrine cells, retinal topography, superior-inferior maturation, tyrosine hydroxylase

Recent data from several laboratories suggest that the function of CA amacrine cells is strongly associated with the activity of rod photoreceptor cells (Pourcho, '82; Hamasaki et al., '86; Ikeda et al., '86; Hokoc and Mariani, '87; Voigt and Wässle, '87). The distribution of amacrine cells in the retina may also provide an index of their function. The distribution of CA neurones has now been studied in several species and has proved relatively distinctive (*cats:* Oyster et al., '85; Mitrofanis et al., '88b; *humans:* Mitrofanis and Provis, '89; *rats*: Versaux-Botteri et al., '86; Mitrofanis et al., '88b; *rabbits:* Brecha et al., '84; Negishi et al., '84; Mitrofanis et al., '88b; *opossums:* Kolb and Wang, '85; *monkeys:* Mariani et al., '84; *guinea pigs:* Mitrofanis et al., '88b; *turtles:* Kolb et al., '87). Their distribution is largely independent from that

Accepted September 1, 1989.

Address reprint requests to Dr. B. Finlay, Department of Psychology, Uris Hall, Cornell University, Ithaca, 14583, NY, USA.

A preliminary account of this work has been presented in abstract form (Mitrofanis and Finlay: *Neurosci. Lett.* [Suppl] 30:102, '88).

of the ganglion cells; other amacrine cells; and, except perhaps in the monkey (Mariani et al., '84), the rod photoreceptor cells (Mitrofanis et al., '88b). For example, in cat retinae (Oyster et al., '85; Mitrofanis et al., '88b), CA cells do not concentrate at the area centralis, a region where the density of ganglion cells is highest (Stone, '78). Similarly, the peak density of CA cells is peripheral to any concentration of ganglion cells in rats and guinea pigs (Mitrofanis et al., '88b).

It is noteworthy that other types of amacrine cells also have distinct distributions. For example, the distributions of adrenergic amacrines in rats (Versaux-Botteri et al., '86); nicotinamide adenine dinucleotide phosphate (NADPH) diaphorase amacrines in humans (Provis and Mitrofanis, '89), cats (Wässle et al., '87), rats (Sandell, '85), and guinea pigs (Cobcroft et al., '89); and of somatostatinergic amacrines in rabbits (Sager, '87), cats (Mitrofanis et al., '89c), and humans (Mitrofanis et al., '89c) are distinct from the distributions of retinal ganglion cells in those species. These differences raise interesting questions as to the functional significance of amacrine cell distributions, and of the developmental mechanisms that make them possible.

In this study, we have examined the distribution and cell morphology of CA neurones in adult and developing retinae of Syrian hamsters and Mongolian gerbils. Their changes in distribution during development were then compared to the changes in the distribution of ganglion cells in both species.

We chose these species because, although they are closely related phylogenetically (both of the family Cricetidae), they differ significantly in brain weight (Perez et al., '88), retinal topography (Tiao and Blakemore, '76; Sengelaub et al., '83, '86; Wikler et al., '89), retinal cell number (Sengelaub et al., '86; Wikler et al, '89), and visual acuity (Emerson, '80; Ingle, '81). For example, the topography of the hamster's ganglion cell layer (GCL) is fairly uniform (Sengelaub et al., '83, '86), whereas the GCL of gerbils has a prominent visual streak (Wikler, '87).

MATERIALS AND METHODS

Subjects

Retinae were obtained from Syrian hamsters (*Mesocricetus auratus*) and Mongolian gerbils (*Meriones unguiculatus*) aged P4, P6, P8, P10, P12, P15, P18, P25, and adult. P1 was taken as the day of birth, which in the hamster is the 15.5th post-conceptional day (PCD) and in the gerbil, the 27th PCD. With this criteria, hamster pups open their eyes at P15, and gerbils at approximately P18.

Immunocytochemical procedure

Animals were anaesthetized with urethane and perfused transcardially with 0.1 M phosphate buffer (PB, pH 7.4) followed by 4% buffered paraformaldehyde. The superior surface of each eyeball was marked with a felt pen and later by an incision for orientation. Eyeballs were enucleated and the cornea and lens removed. The eyecups were then immersed in a fresh solution of fixative for approximately 20 minutes. Retinae were dissected free in one piece, washed in phosphate buffered saline (PBS, pH 7.4) containing 1% Triton X-100 (Ajax), and subsequently incubated in i) rabbit serum containing anti-TH (Eugene Tech. Int., 1:2400) for 48 hours at 4°C; ii) biotinylated anti-rabbit Ig (Sigma; 1:1000) for 2 hours at room temperature; iii) the avidin-biotin-peroxidase complex (Sigma; 1:750) for 1 hour at room temperature, and iv) a nickel-enhanced, 3,3-diaminobenzidine (DAB; Sigma) solution (Adams, '81). For control experiments, the anti-TH was replaced by either normal rabbit serum or PBS with the addition of 1% bovine serum albumen (Sigma) and then reacted as above. Control retinae showed no positive immunoreactivity for TH in either species. When reacting postnatal retinae, segments of adult retinae were incubated simultaneously to ensure the effectiveness of the technique. Smaller segments of retinae—segments including regions where the axon layer is thickest, i.e., around the optic disk—were also incubated and compared quantitatively to retinae reacted as a whole. There were no discernible differences in number or distribution between the smaller retinal fragments and retinae reacted as a whole, indicating that antibody penetration was equal across the whole retina. Retinae were laid receptor-side down on gelatinized slides and left to dry overnight at room temperature, to ensure firm adhesion to the slide. They were then dehydrated in ascending alcohols, cleared in xylene, and mounted in Permount. For retinal sections, wholemounts were reacted as before, "sandwiched" between two pieces of filter paper, and dehydrated in ascending alcohols. They were then embedded flat in Paraffin and sectioned on a microtome at 10 μm.

Ganglion cell identification and staining

Nissl staining. After completion of the immunocytochemistry, some retinae were counterstained with cresyl violet as in Stone ('81), thus allowing ganglion cells to be mapped. Retinae were then dehydrated and mounted as before. Ganglion cells were identified according to the criteria set out by Stone ('78).

HRP labelling. Animals were anaesthetized with Nembutal. The skin, bone, and dura mater covering the superior surface of the brain was removed and the retino-recipient nuclei exposed. Approximately 1 μl of HRP (grade 1, lyophilized, Boehringer-Mannheim) was soaked in a small piece of acrylamide gel and implanted into the retino-recipient nuclei of both sides. Approximately 48 hours later, animals were re-anaesthetized and perfused transcardially with 0.1 M PB, followed by 4% paraformaldehyde and 0.5% glutaraldehyde in 0.1 M PB. Eyeballs were enucleated and the retinae dissected free and processed for their HRP content by either the Hanker-Yates reagent (Sigma) or DAB.

Mapping, retinal area, and soma size analysis

Retinae were mapped systematically in 500 μm steps with the aid of a calibrated eyepiece graticule. The data collected are shown as either isodensity, dot, or interpolated maps. Isodensity lines were traced by hand on translucent paper from the original maps and superimposed upon a computer video screen. The isodensity lines were constructed by including values equal to or less than a criterion density inside the isodensity line. The area inside the isodensity line was then shaded to represent the density of the cells: the darker the shading, the higher the density. The dot maps were constructed by using the Magellan programme of Halasz and Martin ('84). For the standardized maps, counts of three retinae were replotted by their radial and circumferential position with respect to the superior rectus and the optic disk in hamsters, and with respect to the visual streak and optic disk in gerbils. In this way, a direct comparison of data at identified topographical points could be made across retinae. No correction was made to the total numbers for shrinkage, since retinae were firmly adherent to the slides before dehydration, presumably limiting shrinkage to less

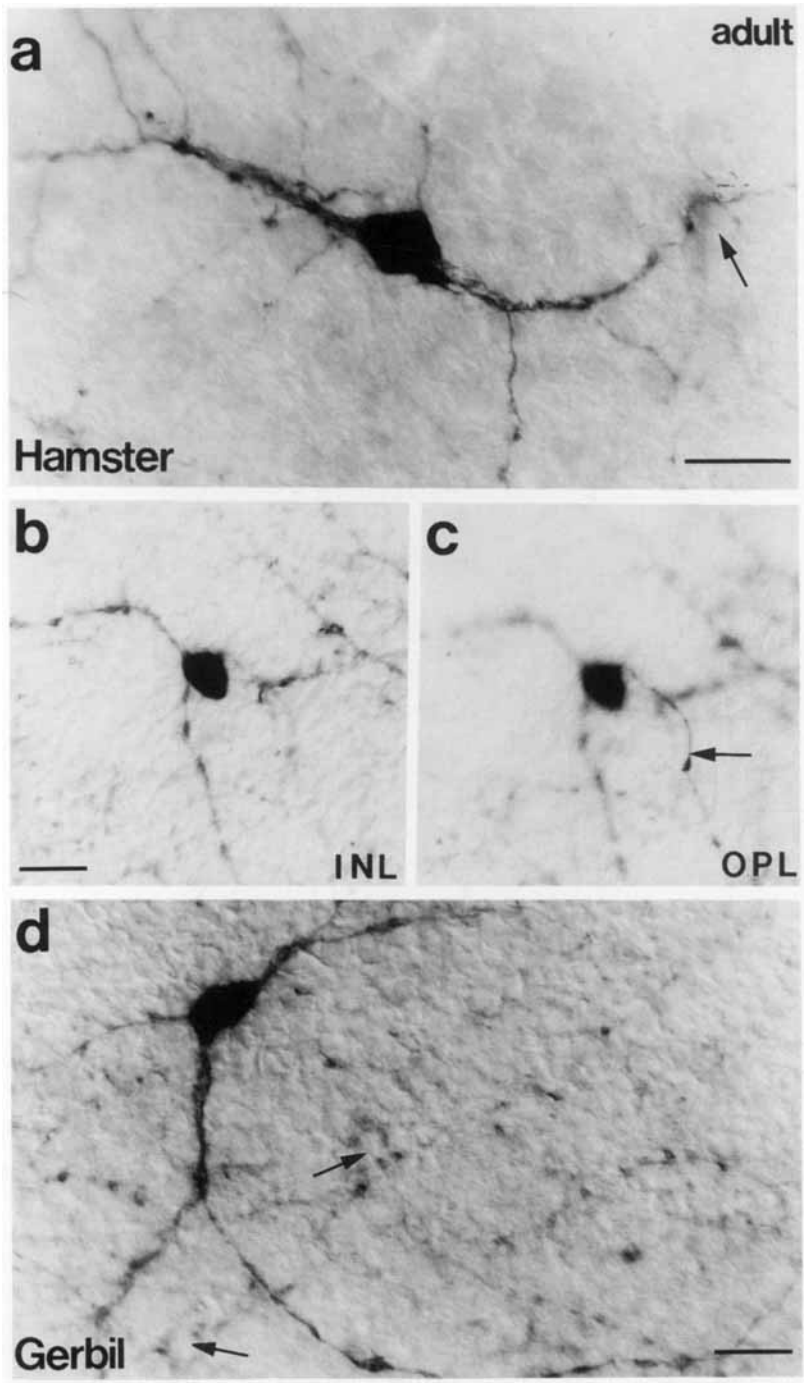

Fig. 1. CA cells in adult hamster (**a,b,c**) and gerbil (**d**) retinae. In hamsters, most somata were in the INL and their dendrites spread in the outer IPL, encircling non-labelled somata (arrow, a). Small numbers of somata in the INL (b) also had a process extending toward the OPL (arrow, c). In gerbils, most somata were in the INL and dendrites in the outer IPL, encircling non-labelled somata (arrowed, d). Cells were photographed with Nomarski optics. Scale = 20 μm.

than 5% (Stone, '81). Analysis of soma size was also undertaken with the Magellan programme. Somata were sampled from the upper temporal and upper nasal margins, as well as from a central region just above the optic disk. Samples of cells were tested for significant differences in their mean soma diameters with a chi-square test.

RESULTS

The morphology of CA cells

Hamsters. The majority of the somata of CA cells in adult hamster retinae were in the inner part of the INL (Fig. 1a) and a minority in either the GCL or IPL (Ballestra et al.,

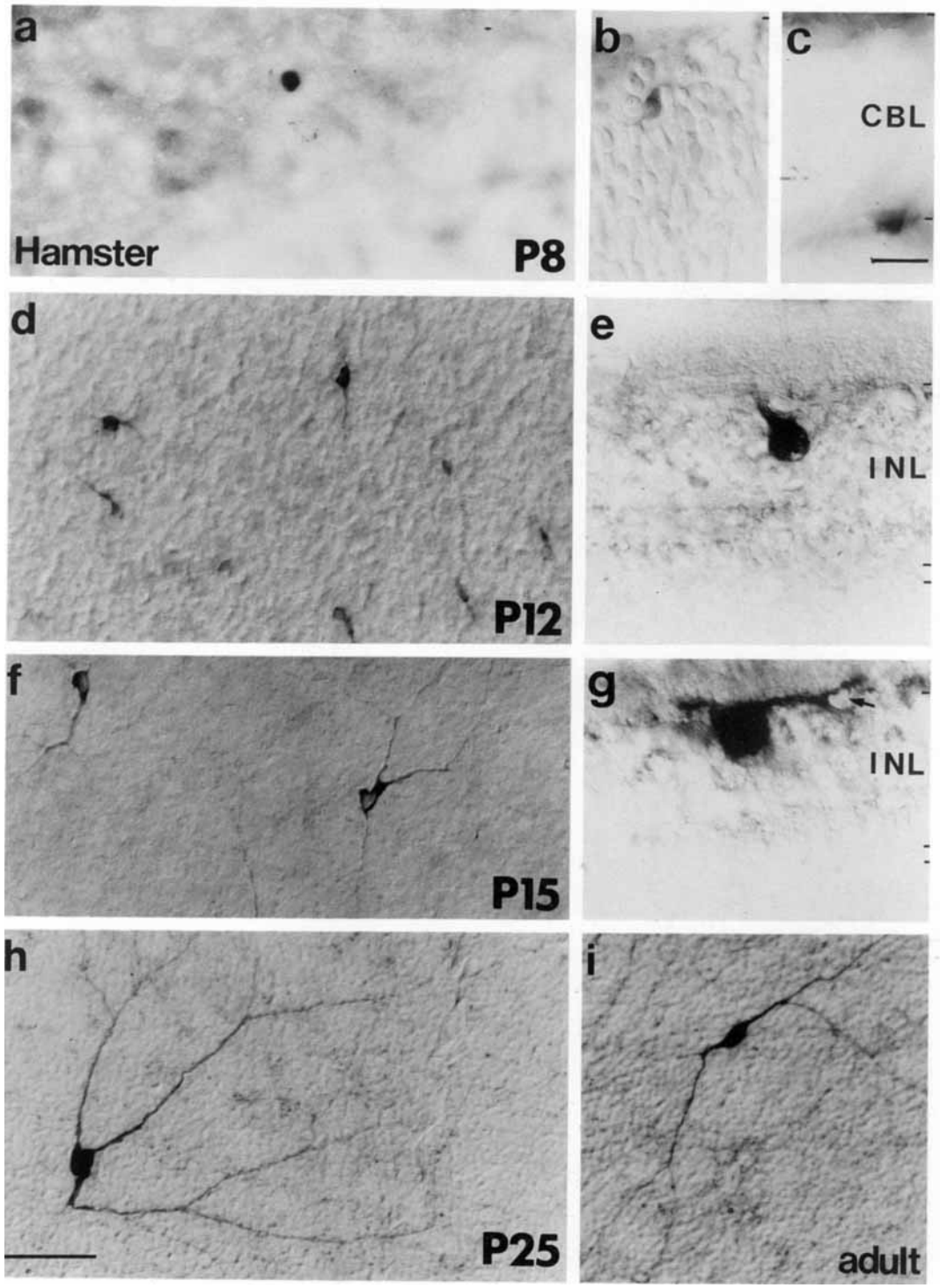

Fig. 2. CA cells in hamster retinae aged P8 (**a,b,c**), P12 (**d,e**), P15 (**f,g**), P25 (**h**) and adult (**i**). See text for descriptive details. Cells were photographed with Nomarski optics. Scale for a,d,f,h,i = 50 μm (in h); Scales for b,c,e,g = 10 μm (in c).

'84). Their diameters averaged 15.2 μm (range, 9–20 μm), which varied significantly ($P < 0.05$) with retinal position, being largest in temporal and smallest in central retina (Fig. 3I). From each soma, several primary dendrites extended into an outer stratum of the IPL (Fig. 1a) and often encircled non-labelled somata (arrowed, Fig. 1a). Small numbers of CA cells with somata in the inner INL (Fig. 1b) also had a process extending in the OPL (arrowed, Fig. 1c), and are probably interplexiform cells.

TH-immunoreactivity was first observed at P8 in either fusiform somata located in the middle of the CBL (Figs. 2a,b), or in rounded somata located in more scleral regions

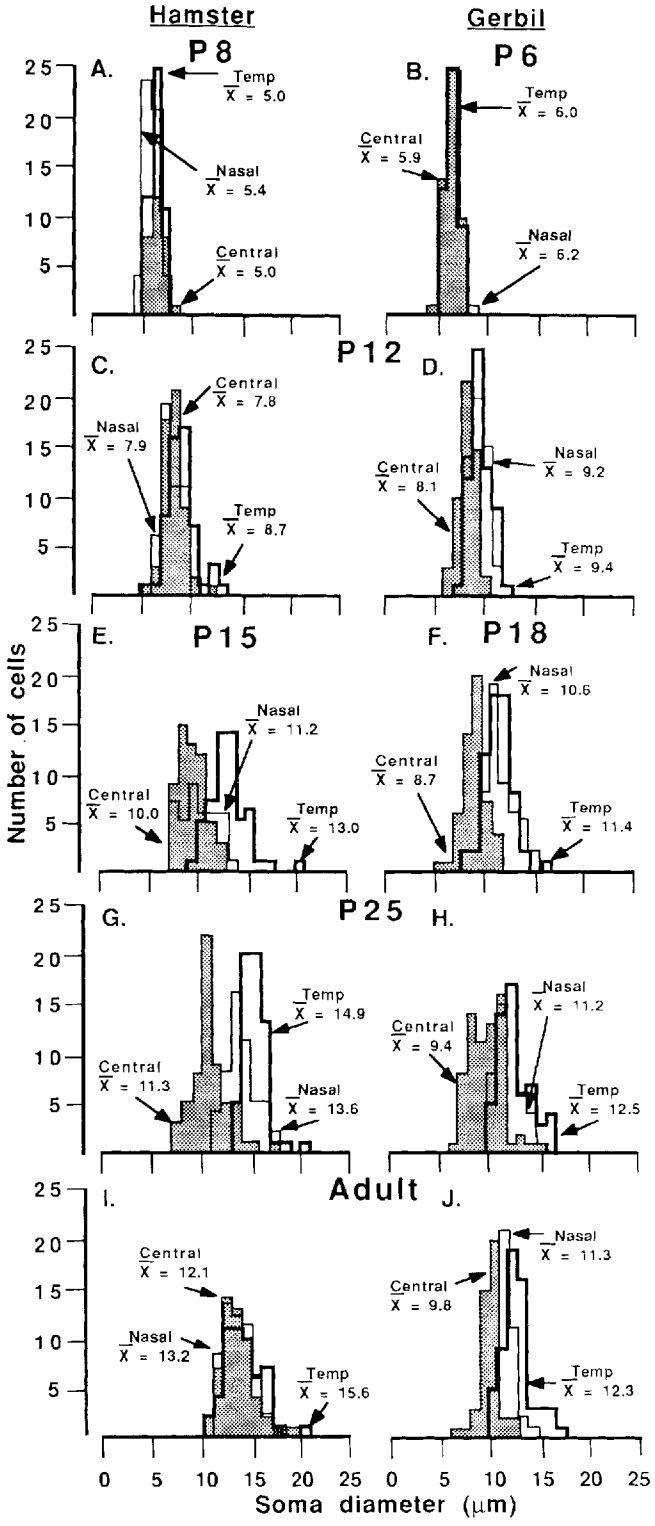

Fig. 3. Frequency × soma diameter histograms of CA cells in adult and developing hamster and gerbil retinae. Somata were sampled from temporal (thick lines), central (shaded) and nasal (thin lines) regions of retina. Sample number ranged from 49 to 60 cells, and SD ranged from 0.6 to 2.0.

of the CBL (Fig. 2c). Their diameters averaged 5.1 μm (range, 4–8 μm), which did not vary significantly ($P > 0.05$) across the retina (Fig. 3A). By P12, CA somata had grown considerably (range, 5–12 μm; mean 8.1 μm). Growth was greatest among temporal (43%) and least among nasal cells (32%) and the resultant soma size gradient was significant ($P < 0.05$; Fig. 3C). At this age, most labelled somata were rounded and found in the inner part of the INL (Figs. 2d,e): CA somata were not detected in scleral regions of the INL. Dendrites were apparent on these cells, extending toward the outer part of the IPL (Figs. 2d,e). By P15, CA dendrites spread in an outer stratum of the IPL and encircled small non-labelled somata (arrowed, Fig. 2g). Their somata at this age averaged 11.4 μm in diameter (range, 7–20 μm). From P12 to P15, soma growth was greatest among temporal and nasal cells, both increasing approximately 20%, as against 14% for central cells (Fig. 3E). At P25, the morphology (Figs. 2h) and soma diameters (Fig. 3G) of CA cells were similar to those in adults.

Gerbils. As in hamsters, most CA somata in adult gerbil retinae were in the inner part of the INL (Fig. 1d). Their diameters averaged 13 μm (range, 6–17 μm), which varied significantly ($P < 0.05$) across the retina, being largest in temporal and smallest in central retina (Fig. 3J). Their dendrites spread into an outer stratum of the IPL and encircled or partially encircled non-labelled somata (arrowed, Fig. 1d). Small numbers of CA somata were also in the GCL or IPL and their dendrites spread in the same plexus in the IPL as those of the somata in the INL. CA interplexiform cells were not detected in gerbils.

TH-immunoreactivity was first observed at P6 in fusiform somata located in the middle of the CBL (Figs. 4a,b). Their diameters averaged 6 μm (range, 4–8 μm), which did not vary significantly ($P > 0.05$) across the retina (Fig. 3B). By P12, CA somata had grown considerably (range, 6–12 μm; mean 8.9 μm) and significant ($P < 0.05$) gradients in diameter were apparent across the retina. Somata were larger in temporal and nasal retina than in central (Fig. 3D), indicating that growth between P6 and P12 was greater among peripheral cells than among central cells (36% and 33% as against 27%). At this age, most CA somata were rounded and located in the inner part of the INL (Figs. 4c,d). A small number were observed in the GCL or IPL. From each soma, dendrites extended into an outer stratum of the IPL (Fig. 4d), and by P18, were seen to encircle smaller, non-labelled somata as in adult retinae. Some cells had thin processes directed towards the axon layer (arrowed, Fig. 4f). At P18, the majority of CA somata were in the inner INL (Fig. 4e) and a minority in either the GCL (Fig. 4f) or IPL. Their diameters averaged 10.2 μm (range, 5–16 μm) and from P12, soma growth was greatest among temporal cells, with an increase of approximately 18%. For central and nasal cells, the increase was 5% and 13%, respectively (Fig. 3F). At P25, the morphology (Figs. 4g) and soma diameters (Fig. 3H) of CA cells were similar to those in adults.

Distribution and number of CA cells

The distribution and number of CA cells was examined in three hamster and gerbil retinae at each postnatal age and in the adult. Figure 5 shows the development of CA cell number and mean density, and the increase in retinal area of hamsters and gerbils. The distribution of cells in typical flatmounts (Figs. 6, 7) and their mean distributions with respect to defined retinal landmarks are both presented (Fig. 8).

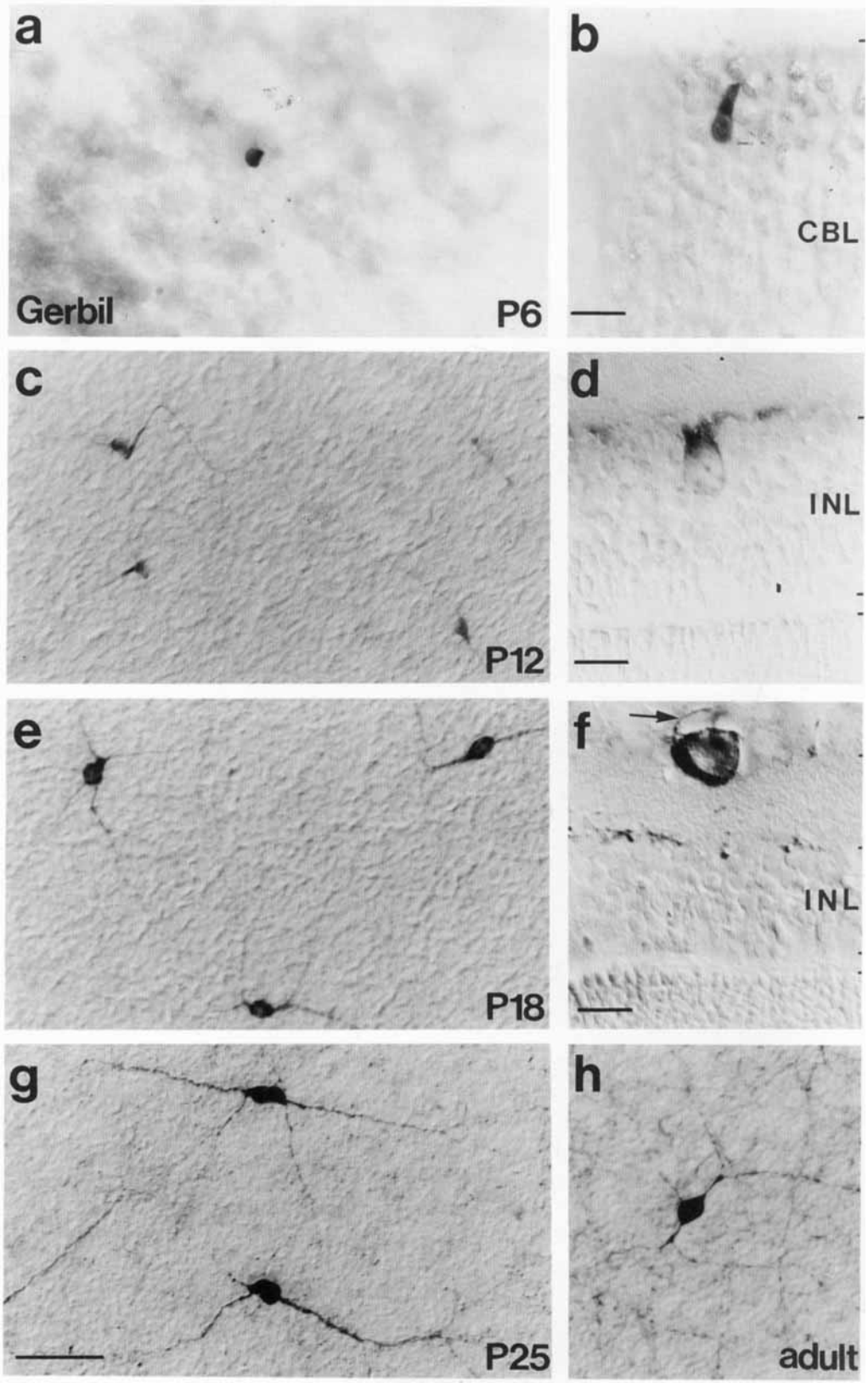

Fig. 4. CA cells in gerbil retinae aged P6 (**a,b**), P12 (**c,d**), P18 (**e,f**), P25 (**g**), and adult (**h**). See text for descriptive details. Cells were photographed with Nomarski optics. Scale for a,c,e,g,h – 50 μm (in g); b,d,f = 10 μm.

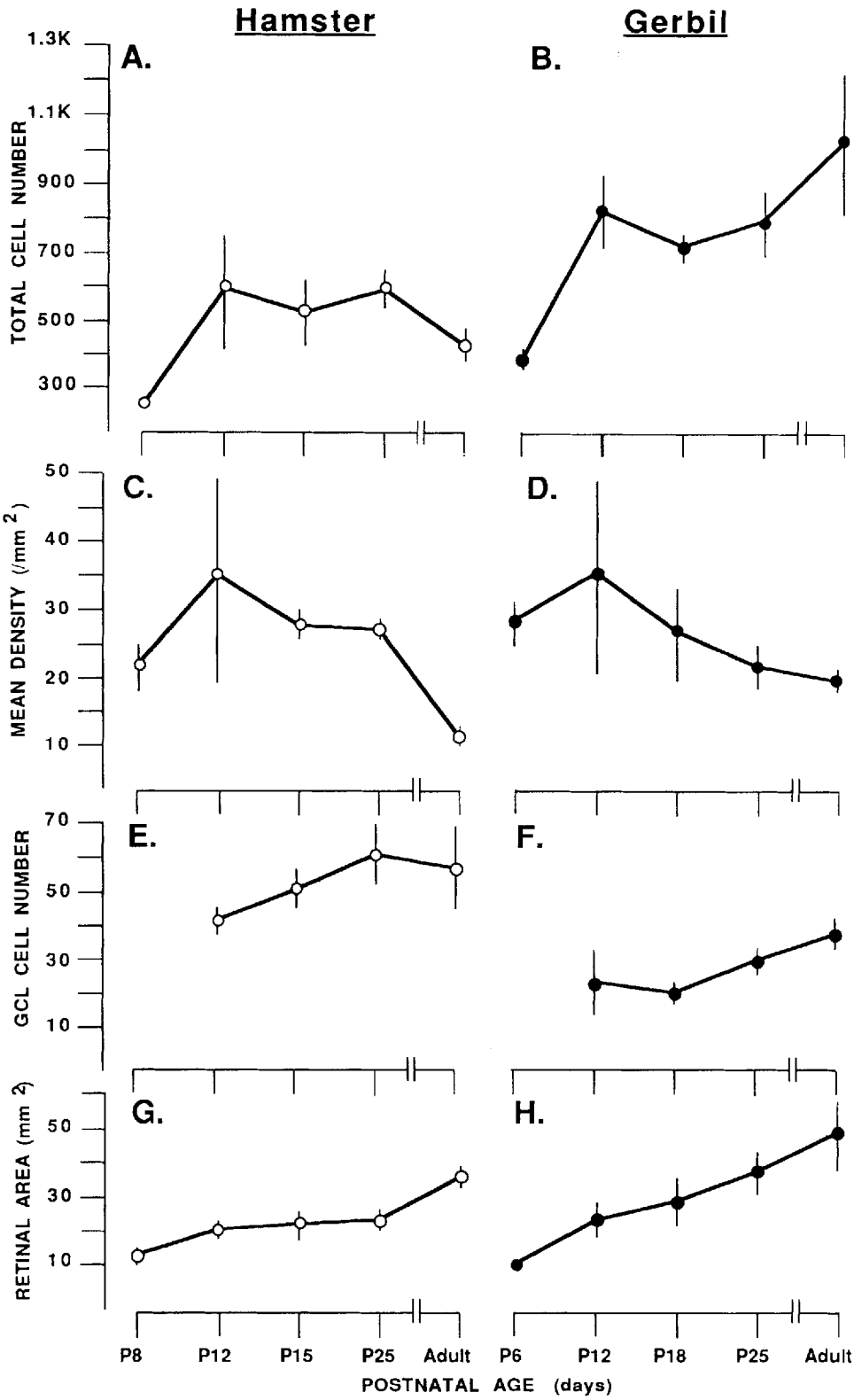

Fig. 5. Graphs of the changes in total number (**A,B**, mean density (**C,D**), and number in the GCL (**E,F**) of CA cells in developing hamster and gerbil retinae. Changes in retinal area of both species are also shown (**G,H**) of CA cells. K = 1,000 cells/mm^2. The plots are mean counts of three different retinae from each postnatal day examined.

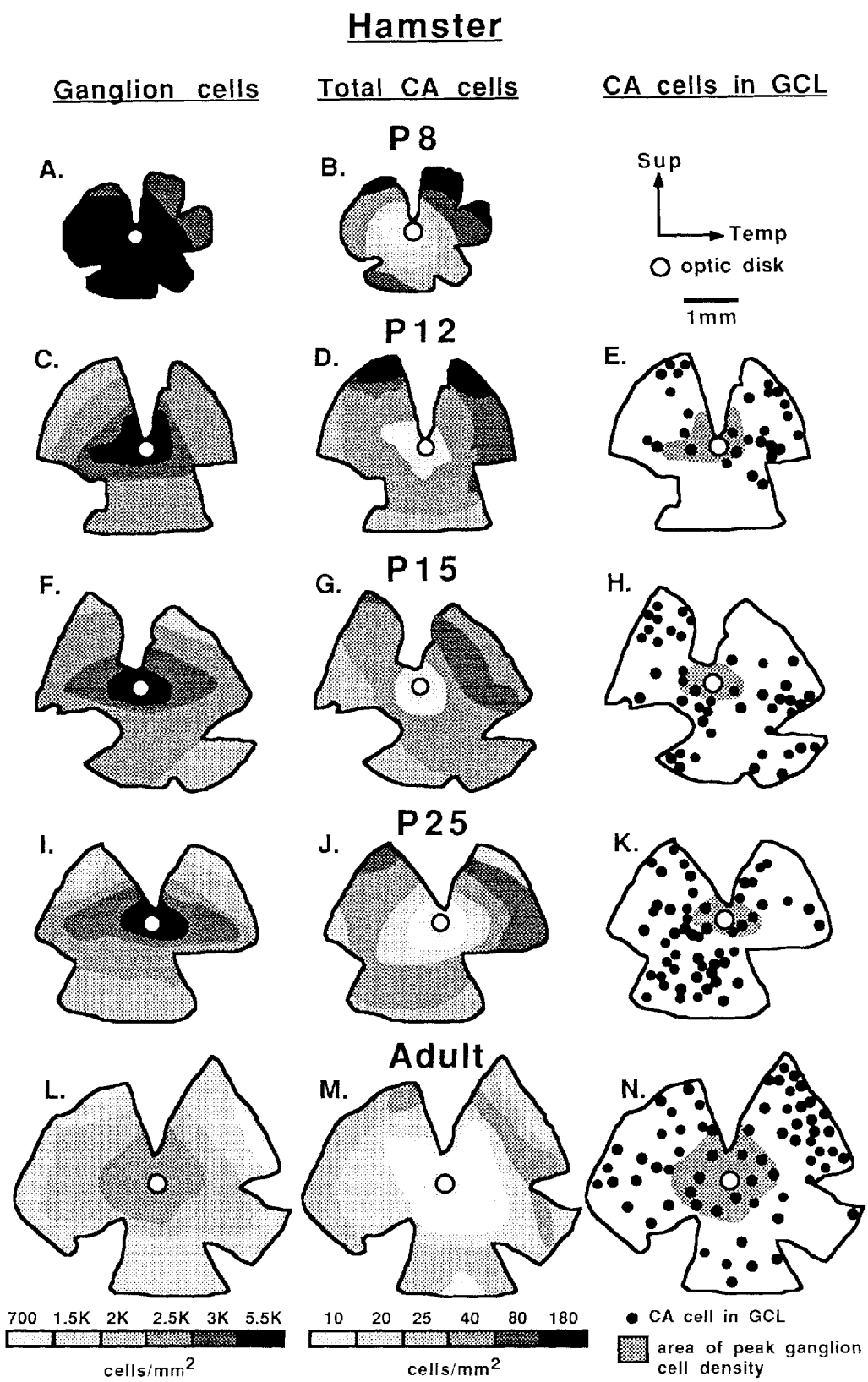

Fig. 6. Maps of the distribution of presumed ganglion cells, total CA cells, and CA cells in the GCL, in the same hamster retina at each postnatal age examined. Note that the density ranges in the adult retina (L) closely match the density ranges of HRP-labelled cells in Figure 8A. K = 1,000 cells/mm^2.

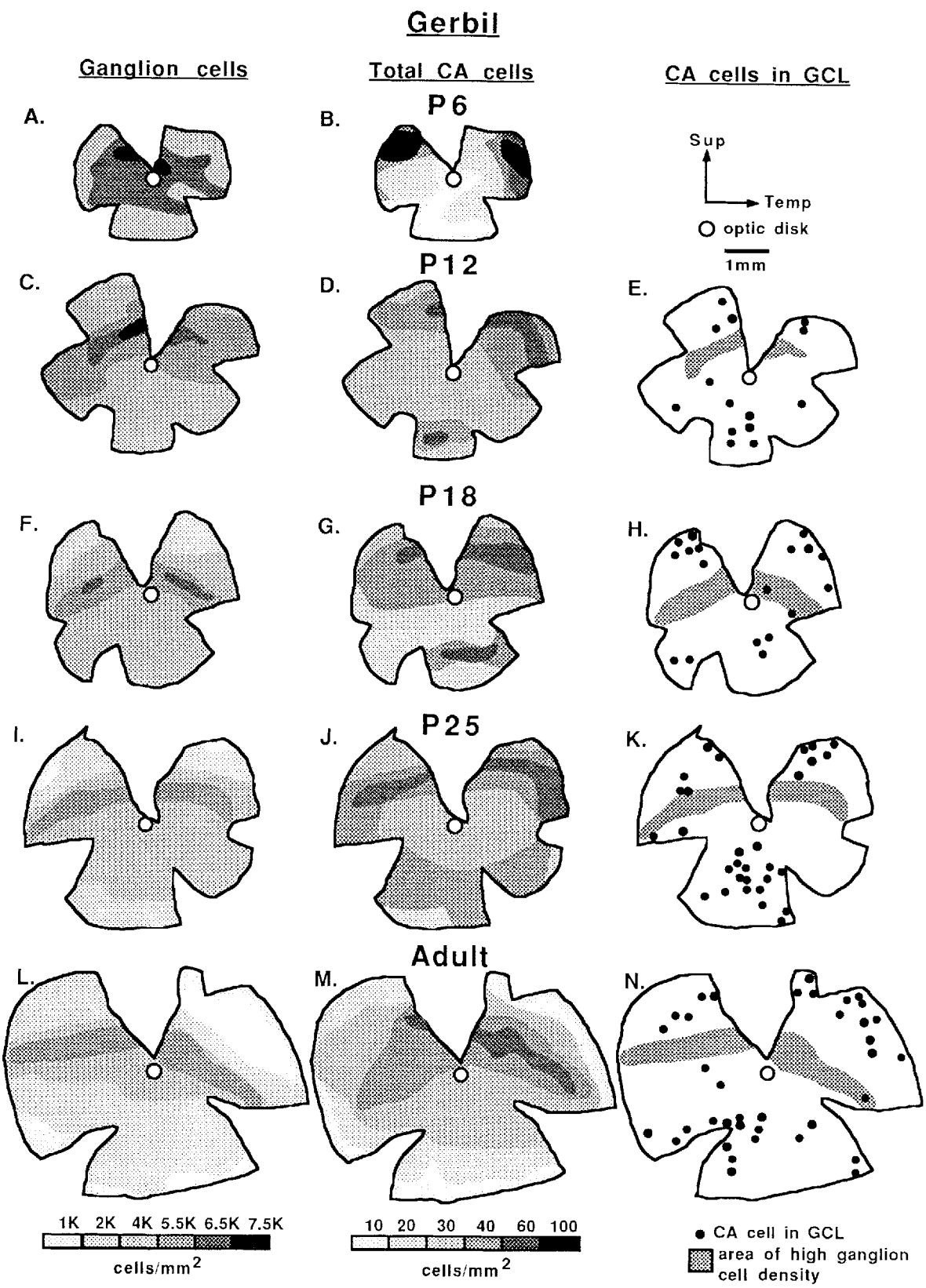

Fig. 7. Maps of the distribution of presumed ganglion cells, total CA cells, and CA cells in the GCL, in the same gerbil retina at each postnatal age examined. Note that the density ranges in the adult retina (L) closely match the density ranges of HRP-labelled cells in Figure 8C. K = 1,000 cells/mm^2.

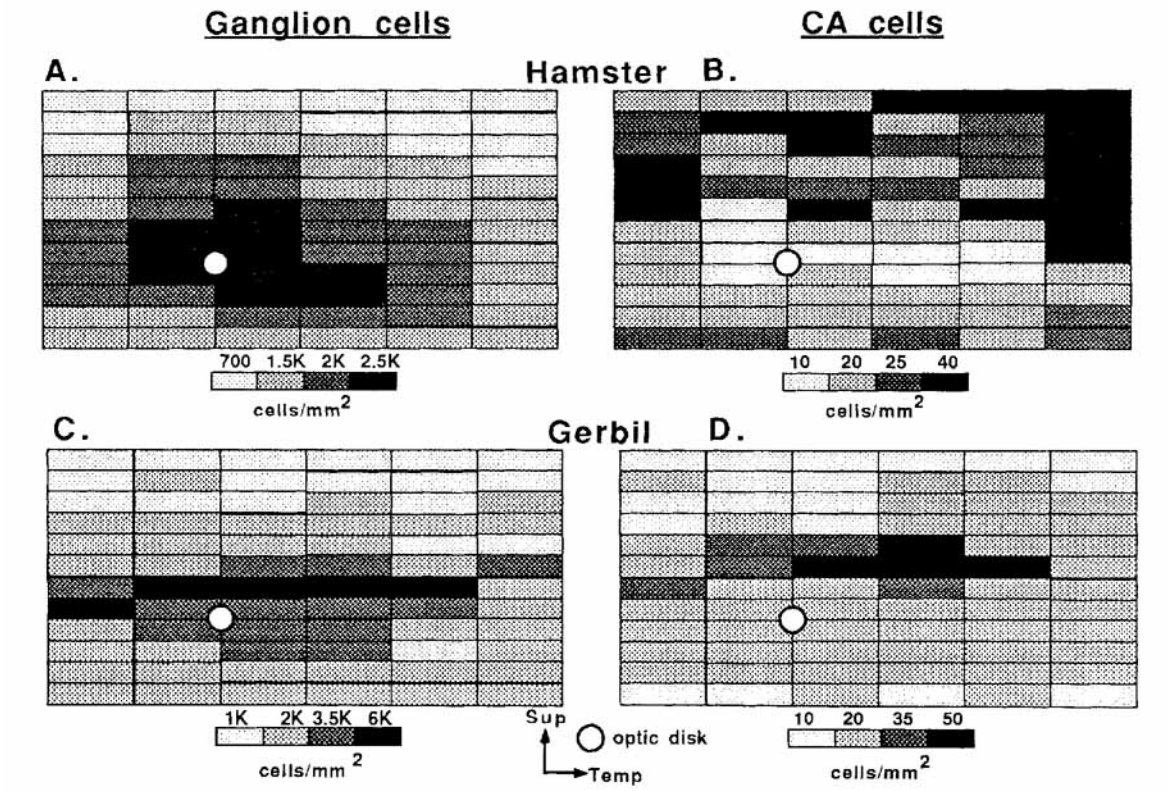

Fig. 8. Interpolated maps of the distributions of ganglion cells (**A,C**) and of CA cells (**B,D**) in adult retinae of hamsters and gerbils. Ganglion cells were identified after retrograde transport of HRP from the retinorecipient nuclei. Their number in hamster retinae ranged from 72,204 to 84,679 (n = 3), confirming the estimates reported by Linden and Esberard ('87). In gerbil retinae, their number ranged from 100,137 to 117,176 (n = 3), confirming the estimates reported by Wikler et al. ('89). K = 1,000 cells/mm^2.

Hamsters. Total CA cell number in adult hamster retinae averaged 438, with a mean density of 12/mm^2 (Table 1). Density was maximal in superior temporal retina (36/mm^2) and minimal in a broad area around the optic disk (4/mm^2; Figs. 6M, 8B). This area of low density was presumably not due to inadequate penetration of the antibody, since smaller fragments of retina also had minimal densities in this area. CA cells in the GCL numbered 55, forming 13% of the total CA cell number (Table 1). The distribution of CA cells in this layer was relatively uniform (Fig. 6N).

The distribution of ganglion cells in adult hamsters was markedly different from the distribution of CA cells. Ganglion cells concentrated in a broad area centered around the optic disk and density was generally higher in inferior than in superior retina (Figs. 6L, 8A). Density ranged from 2,500/mm^2 in central retina to 450/mm^2 in the superior periphery. These results confirm those of Sengelaub et al. ('83).

At P8, a distinct concentration was observed among CA cells at the superior margin. In central and most of inferior retina, very few cells were evident (Fig. 6B). By contrast, the density of presumed ganglion cells at this age was relatively uniform (Fig. 6A). The number of CA cells at this age averaged 251, with a mean density of 21/mm^2 (Table 1). Density ranged from 109/mm^2 in superior to 4/mm^2 in central retina (Table 1). By P12, CA cell density had increased in inferior retina, but clear areas of high density were still apparent at the superior margin. Minimal densities were found around the optic disk (Fig. 6D). The distribution of presumed ganglion cells, on the other hand, was almost inverse to that of the CA cells, with a peak in density in central retina (Fig. 6C). At P12, the number of CA cells increased considerably from P8, averaging 611. Mean density was 35/mm^2, ranging from 191/mm^2 in superior to 5/mm^2 in central retina (Table 1). At P15, peak CA cell density was more localized within superior temporal retina and closer to the optic disk and areas of low density were again evident in central retina (Fig. 6G). The number of CA cells at this age was slightly lower than at P12, averaging 472 (Table 1). Mean density was 27/mm^2, ranging from 81/mm^2 in superior to 7/mm^2 in central retina (Table 1). At P25, the distribution of CA cells resembled that of the adult, except that density was higher in the periphery (Fig. 6J). The number of CA cells at this age was similar to that at P15, but higher than in adults, averaging 589 (Table 1). Mean density was 27/mm^2, ranging from 56/mm^2 in superior to 9/mm^2 in central retina (Table 1).

In the GCL, the number of CA cells increased from an average of 41 at P12 to adult values of 60 at P25 (Table 1). In distribution, labelled cells in this layer at P12 were mostly found in superior retina (Fig. 6E), but by P15, they were located in all retinal regions (Fig. 6H), as in adults (Fig. 6N).

Gerbils. In adult gerbil retinae, CA cells concentrated in an area extending almost horizontally across the retina, superior to the concentration of ganglion cells. Peak density

TABLE 1. CA Cells in the Retina of the Hamster

Retina	Area (mm^2)	No. Total cells	No. INL cells	No. GCL cells	% GCL	RANGE (/mm^2)	C:P ratio	XD (/mm^2)
P8								
8H1	14	240	240	—	—	4–92	1:23	18
8H2	12	258	258	—	—	4–100	1:25	21
8H3	10	256	256	—	—	4–136	1:34	25
Mean	12	251	251 (CBL)	—	—	4–109	1:27	21
P12								
12H1	22	414	376	38	12	8–180	1:23	19
12H2	16	757	712	45	16	4–228	1:57	47
12H3	17	662	621	41	17	4–164	1:41	38
Mean	18	611	570	41	18	5–191	1:38	35
P15								
15H1	24	616	570	46	9	8–68	1:9	26
15H2	15	377	345	32	10	8–84	1:21	26
15H3	14	422	366	56	15	8–92	1:12	30
Mean	18	472	427	45	11	7–81	1:11	27
P25								
25H1	24	644	573	71	11	8–60	1:8	27
25H2	23	580	524	56	10	12–56	1:5	26
25H3	20	542	489	53	10	8–52	1:7	27
Mean	22	589	529	60	10	9–56	1:6	27
Adult								
AH1	37	376	323	53	14	4–32	1:8	10
AH2	38	481	420	61	14	4–36	1:9	13
AH3	36	456	412	44	10	4–40	1:10	13
Mean	37	438	383	55	13	4–36	1:9	12

TABLE 2. CA Cells in the Retina of the Gerbil

Retina	Area (mm^2)	No. Total cells	No. INL cells	No. GCL cells	% GCL	Range (/mm^2)	C:P ratio	XD (/mm^2)
P6								
6G1	16	418	418	—	—	8–96	1:12	27
6G2	15	469	469	—	—	4–84	1:21	31
6G3	15	381	381	—	—	4–76	1:19	25
Mean	15	423	423 (CBL)	—	—	5–85	1:17	28
P12								
12G1	27	717	703	14	2	16–52	1:3	26
12G2	31	716	700	16	2	12–56	1:5	33
12G3	19	923	889	34	4	32–116	1:4	50
Mean	27	785	764	21	3	20–73	1:4	30
P18								
18G1	30	705	690	18	3	12–52	1:4	24
18G2	34	686	665	21	3	12–52	1:4	20
18G3	23	760	738	22	3	12–68	1:6	33
Mean	29	717	697	20	3	12–57	1:5	27
P25								
25G1	42	880	847	33	4	12–52	1:4	21
25G2	36	694	668	26	4	8–48	1:6	19
25G3	32	792	765	27	3	12–56	1:5	25
Mean	37	789	760	29	4	11–52	1:5	22
Adult								
AG1	58	1228	1195	33	3	4–44	1:11	21
AG2	52	991	949	42	4	4–44	1:11	19
AG3	40	803	768	35	4	8–52	1:7	21
Mean	50	1007	970	37	4	5–47	1:9	20

was in superior temporal retina, in an area midway between the optic disk and superior temporal margin (Figs. 7M, 8D). The total number of CA cells averaged 1,007 (Table 2), with a mean density of 20/mm^2, ranging from 5/mm^2 at the superior edge to 47/mm^2 just above the visual streak in temporal retina (Table 2; Figs. 7M, 8D). In the GCL, CA cells numbered 37 and formed approximately 4% of the total CA cell population (Table 2). In distribution, most CA cells in this layer were located in the periphery (Fig. 7N).

Ganglion cells in adult gerbils peaked in density in an elongated area just superior to the optic disk. Density ranged from 200/mm^2 in the superior periphery to 5,500/mm^2 in the visual streak (Fig. 8C). Density was fairly uniform across the visual streak, with no clear evidence of a localized peak in temporal retina. Density was generally higher in inferior than superior retina. These results are similar to those of Wikler et al. ('89).

CA cells at P6 were largely confined to the superior retinal margins (Fig. 7B), whereas the density of ganglion-like cells peaked in a broad area around the optic disk (Fig. 7A). At this age, the number of CA cells averaged 423 (Table 2). Mean density was 28/mm^2, ranging from 85/mm^2 in superior to 5/mm^2 in inferior retina (Table 2). By P12, the area of peak CA cell density was more localized in superior temporal retina and density in inferior retina had increased substantially (Fig. 7D). Ganglion-like cells at P12 peaked in

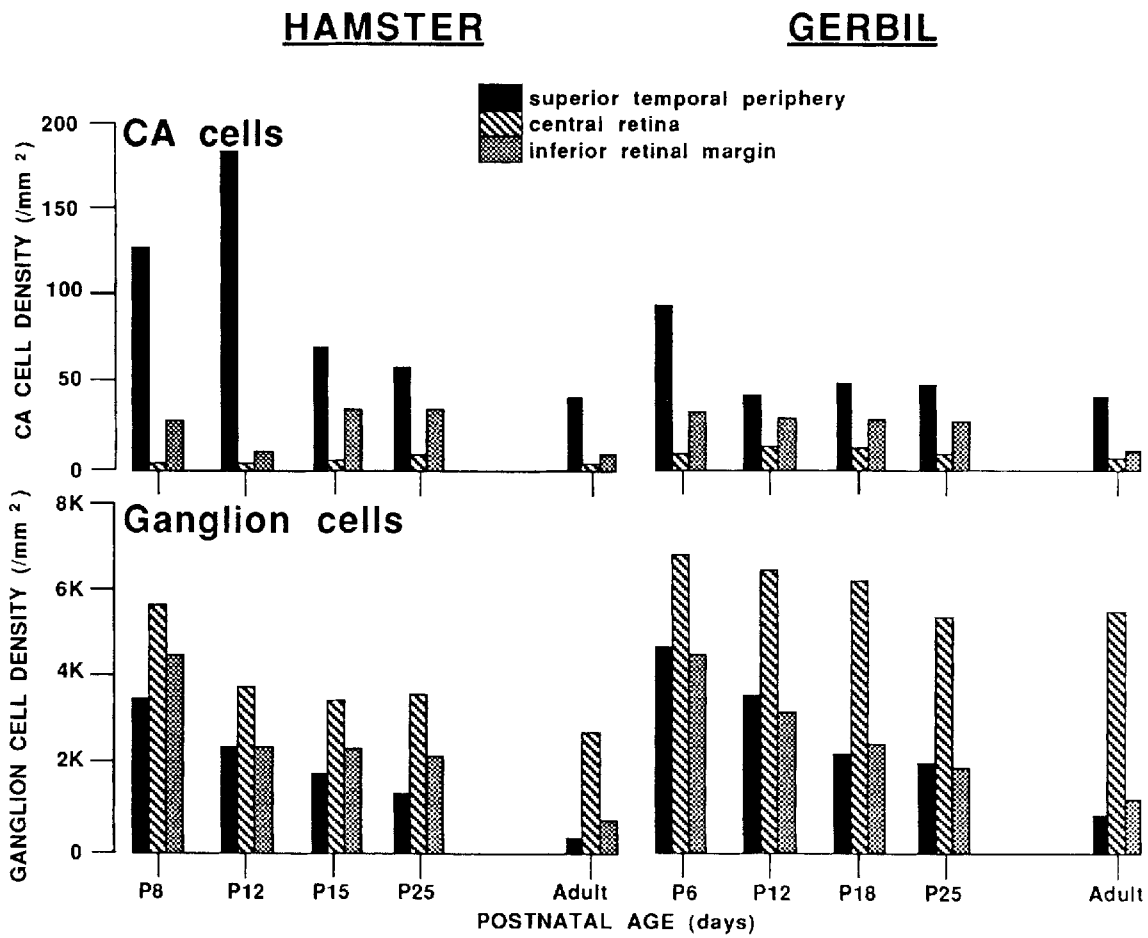

Fig. 9. Graphs of the changes in density of CA and of ganglion cells during development. Densities indicated at each retinal region were the average of at least four adjacent 1 mm samples and values for both classes of cells were from the same retinae at each age. K = 1,000 cells/mm^2.

density in an elongated area just above the optic disk (Fig. 7C). At this age, the number of CA cells almost doubled from P6 to a mean of 785 (Table 2). Mean density was 30/mm^2, ranging from 73/mm^2 in superior to 20/mm^2 in inferior retina (Table 2). By P18, the area of peak CA cell density was situated closer to the optic disk than at P12 (Fig. 7G). Their number was similar to P12, averaging 717 (Table 2). Mean density was 27/mm^2, ranging from 57/mm^2 in superior to 12/mm^2 in inferior retina (Table 2). By P25, the distribution of CA cells was almost adult-like, except that density was higher in the periphery (Fig. 7J). At this age, their number averaged 789 (Table 2). Mean density was 22/mm^2, ranging from 52/mm^2 in superior to 11/mm^2 in inferior retina (Table 2).

In the GCL, the number of CA cells continued to increase from an average of 21 at P12 to 37 by adulthood (Table 2). In distribution, labelled cells in this layer at P12 were located in the retinal periphery (Fig. 7E), as in the adult (Fig. 7N).

Comparison of CA and ganglion cell densities during development

Figure 9 shows the changes in density among CA and presumed ganglion cells during development at the superior temporal periphery (area of peak CA cell density), central retina (area of peak ganglion cell density) and the inferior retinal margin. Densities indicated at each retinal region were the average of at least four adjacent 1 mm samples and the values used for both classes of cells were from the same retinae at each age.

Hamsters

Superior temporal periphery. From P8 to P12, the density of CA cells in this region increased by 25%, whereas the density of presumed ganglion cells decreased by 40%. From P12 to P15, the densities of CA and of presumed ganglion cells both decreased, with the decrease being greatest among CA cells (62% as against 18%). From P15 till adulthood, the densities of CA and of ganglion cells declined by approximately the same proportion (47% and 58%, respectively).

Central retina. Except for a period between P12 and P25 where it increased slightly, CA cell density stayed relatively stable during development. Conversely, the density changes of presumed ganglion cells in this region were also minimal.

Inferior retina. From P8 to P12, the densities of CA and of presumed ganglion cells in this region decreased by approximately the same proportion (66% as compared with 51%). From P12 to P15, however, the density of CA cells

increased by 71% whereas the density of ganglion cells underwent no significant change. From P15 till adulthood, the densities of CA and of ganglion cells declined by the same proportion (57% and 61%, respectively).

Gerbils

Superior temporal periphery. From P6 to P12, the density of CA cells in this region decreased by 54%, whereas the density of presumed ganglion cells decreased by only 29%. From P12 till adulthood, the density of CA cells changed little, whereas the density of ganglion cells declined by 73%.

Central retina. The densities of CA and of presumed ganglion cells stayed relatively stable during development in this region.

Inferior retina. From P6 to P25, the density of CA cells stayed relatively the same, but the density of presumed ganglion cells declined by 58%. From P25 till adulthood, the densities of CA and of ganglion cells declined by the same proportion (50% and 41%, respectively).

DISCUSSION

We have examined CA neurones in adult and developing retinae of hamsters and gerbils by means of TH-immunocytochemistry. This technique demonstrated cells only after they expressed TH and our analysis of their distribution considered changes in maturational expression of TH, cell death and retinal growth. We also compared the developmental changes in the distribution of CA cells to those of presumed ganglion cells. In adult retinae, ganglion cells were identified after retrograde transport of HRP injected into the retino-recipient nuclei, whereas in developing tissue (and in some instances, also in the adult), we relied on Nissl staining to distinguish them from other cells in the GCL. This latter method, however, is less reliable for positive identification of ganglion cells, particularly in the developing tissue (see Stone et al., '82; Wong and Hughes, '87; Henderson et al., '88; McCall et al., '87; Robinson et al., '89). Our counts therefore, may be subject to a certain degree of error. Nonetheless, the data generated on their distribution provided a useful comparison with the CA cells.

The emergence of CA cells in hamster and gerbil retinae: comparison with other species

The development of CA cells in mammalian retinae has now been examined in several species, including rats (Nguyen-Legros et al., '83; Mitrofanis et al., '88a; Martin-Martinelli et al., '89), cats (Mitrofanis et al., '89a), and rabbits (Mitrofanis et al., '89b). Although the time course of appearance of retinal CA cells varies greatly between species, the relative timing is strikingly similar. For example, in rats, TH-immunoreactivity is first apparent at P3 (Nguyen-Legros et al., '83; Mitrofanis et al., '88a; Martin-Martinelli et al., '89), at approximately 70% of the *caecal period* (period of "blindness"; Dreher and Robinson, '88). In hamsters and gerbils, CA cells first appear at 74% (P8) and 73% (P6) of the caecal period, respectively. Further, in cat (Mitrofanis et al., '89a) and rabbit (Mitrofanis et al., '89b) retinae, CA cells are first apparent at fairly similar stages of the caecal period, at 82% (E59) and 63% (E27), respectively. Thus, the similarity in the relative timing of the cell generation and cell loss in the mammalian retinofugal pathways (Dreher and Robinson, '88), may be extended to the emergence of TH-immunoreactivity in mammalian retinae. By contrast, the relative timing of the first expression choline acetyl transferase (ChAT) in retinal cells varies substantially between species. For example, in chick retinae (Spira et al., '87), ChAT-immunoreactive (IR) cells first appear at 32% (E6) of the caecal period, whereas in cats (Mitrofanis et al., '89a) and rats (Mitrofanis et al., '88a), they first appear at 78% (E56) and 100% (P15) of the caecal period, respectively. Thus, while the first appearance of CA cells may conform to a common mammalian "timetable," the expression of ChAT in retinal cells does not. The significance of this difference is yet to be determined.

Morphological development of CA cells

In each mammalian species studied, TH-immunoreactivity is initially observed in small somata located in the inner and middle regions of the CBL. With subsequent retinal maturity, they migrate into the innermost regions of the INL and spread their dendrites in the outer strata of the IPL, forming dendritic rings by about the time of eye opening (Nguyen-LeGros et al., '83; Mitrofanis et al., '88a, '89a,b; Martin-Martinelli et al., '89). In developing hamster retinae, unlike other species, TH-immunoreactivity was first observed in two types of somata located in either the middle or in more scleral regions of the CBL. Labelled cells located in scleral regions of the INL were not apparent at later ages, suggesting that they may have either migrated into the inner part of the INL, or been a class of horizontal cell that loses TH-immunoreactivity with retinal maturity, as does GABA-immunoreactivity from horizontal cells in the rabbit (Osborne et al., '86) and mouse (Schnitzer and Rusoff, '84).

In hamster and gerbil retinae, as well as rat (Nguyen-Legros et al., '83; Mitrofanis et al., '88a; Martin-Martinelli et al., '89) and cat (Mitrofanis et al., '89) retinae, soma growth of CA cells was greatest in temporal and least in central retina. The lesser growth of somata in central retina may be at least partially due to the high density of cells in this region restricting the growth of individual somata (Rapaport and Stone, '83). The larger sizes of CA and of ganglion cells in temporal retina (Sengelaub et al., '83; personal observations), on the other hand, may be determined "intrinsically" (Rapaport and Stone, '83).

Changes in the number of CA cells during development

There is considerable evidence that large numbers of amacrine cells in the GCL and INL of the retina die during development (Sengelaub et al., '86; Horsburgh and Sefton, '87; Wikler, '87; Wong and Hughes, '87; Robinson, '88). However, in this study, the overall number of CA cells in both hamsters and gerbils did not reduce during the periods of amacrine cell death that occur during early postnatal life (Sengelaub et al., '86; Wikler, '87), suggesting that they may be excluded from cell death. It is of course possible that considerable numbers of potential CA cells may die before they have they have the opportunity to express TH. These findings concur with those reported in rat (Mitrofanis et al., '88a; Martin-Martinelli et al., '89) and rabbit retinae (Mitrofanis et al., '89b), where no reduction in overall CA cell number is apparent. In cat retinae (Mitrofanis et al., '89a), on the other hand, the number of CA cells declines by about 70% during the period of amacrine cell death (Robinson, '88). It is unclear whether this reduction is due to cell death, or to a loss of immunoreactivity. It should be noted however, that in hamster and gerbil retinae, there appeared to be a small loss of CA cells in superior retina, but the overall numbers were balanced by the appearance of new CA cells in central and inferior retina.

Contributions of cell generation, cell loss, and differential retinal expansion to the developing distribution of CA cells

Our data on the development of the distribution of CA cells in hamster and gerbil retinae suggest that as in rats (Mitrofanis et al., '88a), rabbits (Mitrofanis et al., '88b), and cats (Mitrofanis et al., '89a), its generation requires more than one developmental mechanism. These include patterns of maturational expression of TH, cell loss, and retinal expansion.

From very early postnatal life, the development of the distributions of CA cells and of ganglion cells in hamsters and gerbils was distinct. For example, the appearance of CA cells appeared to follow a superior-inferior progression, whereas during the same period, a concentration of presumed ganglion cells emerged in central retina (see Sengelaub et al., '86; Wikler et al., '89). It is noteworthy that in cat (Mitrofanis et al., '89a) and rat (Mitrofanis et al., '88a) retinae, a similar superior-inferior gradient of CA cell appearance is also apparent. Thus, what factor cause this asymmetrical appearance of CA cells? One possibility is that their appearance reflects the sequence of their generation. However, amacrine cells (as a group) are generated centroperipherally in gerbils (Wikler et al., '89) and uniformly in hamsters (Sengelaub et al., '86). Perhaps CA cells are generated very late during amacrine cell cytogenesis and their initial generation is "displaced" from central retina (where other cells concentrate) to the superior temporal periphery. Indeed, Evans and Batelle ('87) report that dopaminergic amacrine cells of rat retinae are born relatively late during amacrine cell cytogenesis and the same may be true for these cells in gerbils and hamsters. Alternatively, CA cells may be born in a pattern similar to other amacrine cells, and some other mechanism "switches on" the expression of TH in a superior-inferior progression.

Our analysis of the contributions of cell loss in the generation of the distribution of CA cells in hamster and gerbil retinae, suggests that it may only play a minor role. For example, during early development, there was a small loss of CA cells in superior retina and not elsewhere (see Fig. 9). It is difficult to comment on the significance of this loss, since it does not substantially change their distribution. In cat retinae, on the other hand, patterns of cell loss among CA cells significantly change their distribution and is an important determinant in the generation of their distinct distribution (Mitrofanis et al., '89a). It seems unlikely, however, that the patterns of CA cell loss in hamsters and gerbils significantly affect or create their distinct distribution.

As in cat (Mitrofanis et al., '89a) and rabbit (Mitrofanis et al., '89b) retinae, the differential expansion of the retina in hamsters and gerbils appears to contribute to the lowering of peripheral densities of CA cells (and of ganglion cells), especially between P25 and adulthood. The pattern of retinal expansion in gerbils is different from that in hamsters. Before P10, gerbil retinae are elongated along their horizontal axes. From P10 to adulthood, gerbil retinae expand more along their vertical (superior-inferior) than their horizontal (naso-temporal) axes, forming almost hemi-spherical retinae in adults (Wikler et al., '89). This asymmetrical growth is of primary importance in the formation of the gerbil's prominent visual streak (Wikler et al., '89). Similarly, this type of growth may also affect the distribution of CA cells. For example, CA cell density in gerbils declined more at the superior and inferior margins (40–50%), than at either the temporal and nasal margins (10–20%) between P25 and adulthood. Hamster retinae, on the other hand, undergo symmetrical differential expansion with each area of the periphery expanding equally (Sengelaub et al., '86): ganglion cell and CA cell density both decrease by 40–50% in all areas of the periphery between P25 and adulthood. As a consequence, the distribution of CA cells in hamster retinae is not strongly oriented along the horizontal meridian and remains high in the mid-retinal periphery, reflecting its original distribution. In gerbil retinae, the peak of CA cell density is displaced from the superior periphery toward the centre of the retina and made visual streak-like by this asymmetrical growth.

ACKNOWLEDGMENTS

We are indebted to Jonathan Stone for his invaluable assistance during the production of this paper. We thank Jonathan Stone and Stephen Robinson for their critical reading of the manuscript; Ken Wikler and Vincent Tamariz for the many discussions; Martha Windrem, and Gordon Williams, and Clive Jefferey for their excellent technical assistance.

LITERATURE CITED

Adams, J.C. (1981) Heavy metal intensification of DAB-based HRP reaction product. J. Histochem. Cytochem. *29*:775.

Ballestra, J., G. Terenghi, J. Thibault, and J.M. Polak (1984) Putative dopamine-containing cells in the retina of seven species demonstrated by tyrosine hydroxylase immunocytochemistry. Neuroscience *12*:1147–1156.

Brecha, N.C., C.W. Oyster, and E.S. Takahashi (1984) Identification and characterization of tyrosine hydroxylase immunoreactive amacrine cells. Invest. Opthalmol. Vis. Sci. *25*:66–70.

Cobcroft, M.D., T.M. Vaccaro, and J. Mitrofanis (1989) Distinct patterns of distribution among NADPH-diaphorase neurones in the guinea pig retina. Neurosci. Lett., *103*:1–7.

Dreher, B., and S.R. Robinson (1988) Development of the retinofugal pathway in birds and mammals: evidence for a common timetable. Brain Behav. Evol. *31*:369–390.

Emerson, V.F. (1980) Grating acuity of the golden hamster: effects of stimulus orientation and luminance. Exp. Brain Res. *38*:43–52.

Evans, J.A., and B.A. Batelle (1987) Histogenesis of dopamine-containing neurones in the rat retina. Exp. Eye Res. *44*:407–414.

Halasz, P., and P. Martin (1984) A microcomputer based system for semiautomatic analysis of histochemical sections. R. Microscop. Soc. Proc. *19*:312.

Hamasaki, D.I., W.B. Trattler, and A.S. Hajek (1986) Light on depresses and light off enhances the release of dopamine from the cat's retina. Neurosci. Lett. *68*:112–116.

Henderson, Z., B.L. Finlay, and K.C. Wikler (1988) Development of ganglion cell topography in ferret retina. J. Neurosci. *8*:1194–1205.

Hokoc, J.N., and A.P. Mariani (1987) Tyrosine hydroxylase immunoreactivity in the rhesus monkey retina reveals synapses from bipolar cells to dopaminergic amacrine cells. J. Neurosci. *7*:2785–2793.

Horsburgh, G.M., and A.J. Sefton (1987) Cellular degeneration and synaptogenesis in the developing retina of the rat. J. Comp. Neurol. *263*:553–566.

Ikeda, H., T.D. Priest, J. Robbins, and K. Wakakuwa (1986) Silent dopaminergic synapse at feline retinal ganglion cells? Clin. Vision Sci. *1*:25–38.

Ingle, D.J. (1981) New methods for analysis of vision in gerbils. Behav. Brain Res. *3*:151–175.

Kolb, H., and H.H. Wang (1985) The distribution of photoreceptors, dopaminergic amacrine cells and ganglion cells in the retina of the North American opossum (*Didelphis virginiana*). Vision Res., *25*:1207–1221.

Kolb, H., C. Cline, H.H. Wang, and N. Brecha (1987) Distribution and morphology of dopaminergic amacrine cells in the retina of the turtle (*Pseudemys scripta elegans*). J. Neurocytol. *16*:577–588.

Linden, R., and C.E.L. Esberard (1987) Displaced amacrine cells in the ganglion cell layer of the hamster. Vision Res. *27*:1071–1076.

McCall, M.J., S.R. Robinson, and B. Dreher (1987) Differential retinal growth appears to be the primary factor producing the ganglion cell density in the rat. Neurosci. Lett. *79*:78–84.

Martin-Martinelli, E., A. Simon, A. Vigny, and J. Nguyen-Legros (1989) Postnatal development of tyrosine-hydroxylase immunoreactive cells in rat retina. Morphology and distribution. Dev. Neurosci. *11*:11–25.

Mariani, A.P., H. Kolb, and R. Nelson (1984) Dopamine-containing amacrine cells of rhesus monkey retina parallel rods in spatial distribution. Brain Res. *322*:1–7.

Mitrofanis, J., and B.L. Finlay (1988) Relationship between ganglion cells and catecholaminergic amacrine cells in the adult and developing retinae of the hamster and gerbil. Neurosci. Lett. [Suppl.] *30*:102.

Mitrofanis, J., J. Maslim, and J. Stone (1988a) Catecholaminergic and cholinergic neurones in the developing retina of the rat. J. Comp. Neurol. *276*:343–359.

Mitrofanis, J., A. Vigny, and J. Stone (1988b) The distribution of catecholaminergic cells in the retinas of the rat, guinea pig, cat and rabbit: independence from ganglion cell distribution. J. Comp. Neurol. *267*:1–14.

Mitrofanis, J., and J.M. Provis (1989) A Unique soma size gradient among catecholaminergic neurones of human retinae. Brain Res. (submitted).

Mitrofanis, J., J. Maslim, and J. Stone (1989a) Catecholaminergic and cholinergic neurones in the developing cat retina. Neurosci. Lett. [Suppl.] *34*:S122.

Mitrofanis, J., S.R. Robinson, and K.W.S. Ashwell (1989b) Catecholaminergic neurones in the developing rabbit retina. Neurosci. Lett. [Suppl.] *34*:123.

Mitrofanis, J., S.R. Robinson, and J.M. Provis (1989c) Somatostatinergic neurones of the developing human and cat retinae. Neurosci. Lett. *104*:209–216.

Negishi, K., T. Teranishi, and S. Kato (1984) Regional density of monoamine-accumulating amacrine cells in the rabbit retina. Neurosci. Lett. *45*:27–32.

Nguyen-LeGros, J., A. Vigny, and M. Gay (1983) Postnatal development of TH-like immunoreactivity in the rat retina. Exp. Eye Res. *37*:23–32.

Osborne, N.N., S. Patel, D.W. Beaton, and V. Neuhoff (1986) GABA neurones in retinas of different species and their postnatal development in situ and in culture in the rabbit retina. Cell Tissue Res. *243*:117–123.

Oyster, C.W., E.S. Takahashi, M. Cilluffo, and N.C. Brecha (1985) Morphology and distribution of TH-like immunoreactive neurones in the cat retina. Proc. Natl. Acad. Sci. USA *82*:6335–6339.

Perez, G.M., D.R. Sengelaub, K.C. Wikler, and B.L. Finlay (1988) Generation of species differences in eye and brain conformation: allometric and neurogenetic studies. Soc. Neurosci. Abs. *14*:1113.

Pourcho, R.G. (1982) Dopaminergic amacrine cells in the cat retina. Brain Res. *252*:101–109.

Provis, J.M., and J. Mitrofanis (1989) NADPH-diaphorase neurones have a uniform distribution in human retinae. Neurosci Lett. (submitted).

Rapaport, D.H., and J. Stone (1983) Time course of morphological differentiation of cat retinal ganglion cells. J. Comp. Neurol. *221*:42–52.

Robinson, S.R. (1988) Cell death in the inner and outer nucleur layers of the developing cat retina. J. Comp. Neurol. *267*:507–515.

Robinson, S.R., B. Dreher, and M.J. McCall (1989) Non-uniform retinal expansion during the formation of the rabbit's visual streak: implications for the ontogeny of mammalian retinal topography. Visual Neurosci. *2*:201–219.

Sager, S.M. (1987) Somatostatin-like immunoreactive material in the rabbit retina: immunohistochemical staining using monoclonal antibodies. J. Comp. Neurol. *266*:291–299.

Sandell, J.H. (1985) NADPH-diaphorase cells in the mammalian inner retina. J. Comp. Neurol. *238*:466–472.

Schnitzer, J., and A.C. Rusoff (1984) Horizontal cells of the mouse retina contain glutamic acid decarboxylase-like immunoreactivity during early stages of development. J. Neurosci. *4*:2948–2955.

Sengelaub, D.R., M.S. Windrem, and B.L. Finlay (1983) Increased cell number in the adult hamster retinal ganglion cell layer after early removal of one eye. Exp. Brain Res. *52*:269–276.

Sengelaub, D.R., R.P. Dolan, and B.L. Finlay (1986) Cell generation, death and retinal growth in the development of the hamster retinal ganglion cell layer. J. Comp. Neurol. *246*:527–543.

Spira, A.W., T.J. Millar, I. Ishimoto, M.L. Epstein, C.D. Johnson, J.L. Dahl, and I.G. Morgan (1987) Localization of choline acetyl transferase-like immunoreactivity in the embryonic chick retina. J. Comp. Neurol. *260*:526–538.

Stone, J. (1981) The Wholemount Handbook. Sydney, Australia: Maitland.

Stone, J., D.H. Rapaport, R. Williams, and L. Chalupa (1982) Uniformity of cell distribution in the ganglion cell layer of the prenatal cat retina: implications for mechanisms of retinal development. Dev. Brain Res. *2*:231–242.

Stone, J. (1978) The number and distribution of ganglion cells in the cat's retina. J. Comp. Neurol., *180*:753–772.

Tiao, Y.C., and C. Blakemore (1976) Regional specialization in the golden hamster's retina. J. Comp. Neurol. *168*:439–458.

Versaux-Botteri, C., E. Martin-Martinelli, J. Nguyen-LeGros, M. Geffard, A. Vigny, and L. Denoroy (1986) Regional specialization of the rat retina: catecholaminergic-containing amacrine cell characterization and distribution. J. Comp. Neurol. *243*:422–433.

Voigt, T., and H. Wässle (1987) Dopaminergic innervation of AII amacrine cells in mammalian retina. J. Neurosci. *7*:4115–4128.

Wässle, H., M. Hoon Chun, and F. Müller (1987) Amacrine cells in the ganglion cell layer of the cat retina. J. Comp. Neurol. *265*:391–408.

Wikler, K.C., G. Perez and B.L. Finlay (1989) Duration of retinogenesis: its relationship to retinal organization in two cricetine rodents. J. Comp. Neurol. *285*:157–176.

Wong, R.O.L., and A. Hughes (1987) Developing neuronal populations of the cat retinal ganglion cell layer. J. Comp. Neurol. *262*:473–495.